Journal of Magnetic Resonance **156,** 122–130 (2002)
doi:10.1006/jmre.2002.2544

Water Content Profiles with a 1D Centric SPRITE Acquisition

I. V. Mastikhin, H. Mullally, B. MacMillan, and B. J. Balcom[1]

MRI Centre, Department of Physics, University of New Brunswick, P.O. Box 4400, Fredericton, Canada E3B 5A3

Received November 20, 2001; revised April 1, 2002

The purpose of this work is to develop a rapid MRI method amenable to profiling with minimal or no T_1 relaxation weighting. The behavior of a signal during a centric SPRITE acquisition is analyzed. It is shown that the technique can be made immune to a broad range of T_1 changes. In a properly executed measurement, only T_2^* and proton density parameters define the image intensity. A T_2^* mapping technique can be easily applied, separating T_2^* and proton density contributions to the image. A drying soil sample with low initial water content is experimentally studied as a demonstration of the technique. A characteristic baseline artifact is easily removed from the profiles by a simple operation. © 2002 Elsevier Science (USA)

Key Words: **MRI; SPRITE; water content; 1D profiles; porous media.**

1. INTRODUCTION

Magnetic resonance imaging allows direct and noninvasive visualization of static and dynamic water phenomena in porous media. The relaxation times of the water NMR signal in pores are, however, heavily dependent on the strong magnetic susceptibility variations, paramagnetic impurities, and variations of the pore size. MRI is thus a very promising, yet challenging, technique for soil science, and in 1997, the soil science journal *Geoderma* (*1*) published a special issue that dealt solely with the use of NMR and MRI in soil studies.

Conventional MRI methods, developed for use in the medical sciences, cannot easily be applied to studies of solid or semisolid systems. The microscopic heterogeneity of soil leads to effective transverse relaxation, making only a small fraction of the water observable by means of conventional spin echo or gradient echo methods. In addition quantitative information is hard to obtain from an image if the image is distorted by the susceptibility artifacts. As Hall *et al.* stated in (*2*, page 432): "Future studies of soil water should consider the use of other MRI protocols (e.g., for solid state), and measurement at low magnetic fields."

There are several MRI methods developed and successfully applied for studying samples with short relaxation times. Some, such as STRAFI, have been successfully applied to visualize water transport phenomena in various media (*3, 4*). The technique yields a high spatial resolution, but it requires specialized equipment. The STRAFI signal is heavily relaxation weighted, and this weighting can be difficult to unravel in terms of proton density and relaxation time weighting.

An MRI technique ideal for studying fluid content in porous media, such as soils, should be free of artifacts caused by local field inhomogeneities and fast enough to allow for quantitative relaxation measurements in the course of wetting or drying. Quantitative measurement of fluid migration requires the extraction of the proton density data from the experimental image; thus, the impact of different relaxation parameters on the local image intensity must be easily controlled.

We have found that the generic SPRITE technique (single point ramped imaging with T_1-enhancement) (*5*) fits these demands. Preliminary results with a half-k-space variant have been reported (*6, 7*); in this paper we provide a more thorough analysis and demonstration of the technique. The SPRITE technique is a pure phase encoding method and therefore is free from artifacts and distortions due to B_0 inhomogeneities.

The T_1-enhancement, referred to in the name of the technique, is not always desirable, because T_1, in principle, can change significantly during drying or wetting. This would produce variable T_1 weighting, thus hindering the extraction of the true fluid content. We have utilized SPRITE with half-k-space acquisition (*8*) because with this technique the impact of changing T_1 can be easily estimated and avoided. It does not require $5T_1$ delays between excitation pulses and is therefore rapid. The proton density and T_2^* relaxation parameter contributions to the observed image intensity may be separated easily.

2. THEORY

For sequential SPRITE (Fig. 1a), data acquisition starts from the extremity of k-space with maximum gradient value and the center of k-space is sampled when the longitudinal magnetization approaches the steady state, giving the signal intensity

$$S(t = t_p) = M_0 e^{-t/T_2^*} \frac{1 - e^{-\mathrm{TR}/T_1}}{1 - \cos\alpha e^{-\mathrm{TR}/T_1}} \sin\alpha, \qquad [1]$$

where t_p is encoding time, TR is a repetition time, and α is the RF pulse rotation angle.

The centric $1/2$-k-space SPRITE (*8*) pulse sequence is shown in Fig. 1b. The acquisition starts from the center of k-space, when gradients are off, thus acquiring only half of each k-space line.

[1] To whom correspondence should be addressed.

1090-7807/02 $35.00

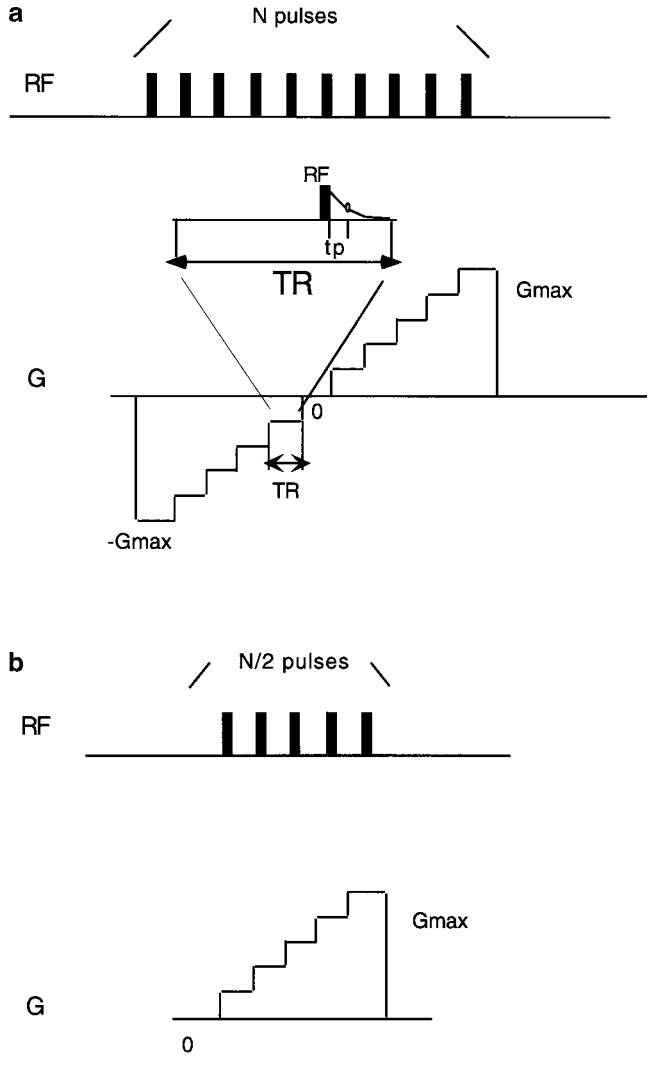

FIG. 1. The pulse sequence for (a) sequential SPRITE and (b) centric SPRITE, where t_p is the phase encoding time, TR is the time between successive RF pulses, and N is the imaging matrix size.

The delays between scans are set to be several T_1's, so the center of k-space is acquired when the longitudinal magnetization starts with the equilibrium value M_0. The signal intensity then is:

$$S(t = t_p) = M_0 e^{-t/T_2^*} \sin\alpha. \qquad [2]$$

The main relaxation parameters that define the SPRITE image intensity are T_2^* and T_1. The T_2^* impact is defined directly by the ratio (t_p/T_2^*) in Eqs. [1] and [2] and can be evaluated by using T_2^*-mapping when both the t_p and the gradient values are systematically varied to keep the field of view constant (*9*). T_1 manifests itself through signal saturation for sequential sampling or through the transient effects for centric sampling.

T_2 does not have a direct impact on the signal intensity for SPRITE. We assume that the transverse magnetization decays completely between two successive pulses. If T_2^* is longer than TR, the transverse magnetization will survive several pulses. In this case, the unwanted transverse magnetization can be removed by the application of an additional gradient spoiler at the origin of k-space (*10*).

For centric acquisition, the longitudinal magnetization can be represented as consisting of two components: a transient component that decays to zero with characteristic time T_{app}, and a steady-state component

$$M_{zn} = M_0(1-w)e^{-\frac{\mathrm{TR}}{T_{app}}n} + M_0 w, \qquad [3]$$

$$\text{where } \frac{1}{T_{app}} = \frac{1}{T_1} - \frac{\ln(\cos\alpha)}{\mathrm{TR}}$$

$$n \text{ is the pulse counter, and steady state } w = \frac{1-E}{1-CE},$$

where $E = \exp(-\mathrm{TR}/T_1)$ and $C = \cos\alpha$. The transient component behaves as an exponential filter on the acquired signal (*8*). After Fourier transformation it becomes a Lorentzian function. This is the point spread function due to evolution of the longitudinal magnetization during sampling. We can call it the *evolution point spread function*; its linewidth is:

$$\Delta x_{EPSF} = \frac{2}{\gamma \Delta G_x T_{app}} \frac{\mathrm{TR}}{t_p}.$$

Comparing it with the sampling point spread function resolution $\Delta x_{SPSF} = (1.2\pi)/(\gamma G_{x\max})$, we find that the transient component causes image blurring when $\Delta x_{EPSF}/\Delta x_{SPSF} > 1$ and the limit on the scanning parameters is:

$$\frac{N}{1.2\pi}\left(\frac{\mathrm{TR}}{T_1} - \ln(\cos\alpha)\right) = 1. \qquad [4]$$

N here is the number of points sampled during the acquisition. This blurring becomes important when the transient component is much larger than the steady-state component w in [3].

During drying or wetting, T_1 can change significantly, and we wish our technique to be immune to these changes. Two different situations should be considered: when TR is much shorter than T_1 and when TR is of the same order as T_1.

2.1. TR Is Much Shorter Than T_1

When TR is much shorter than T_1, it takes a significant amount of time for the sample magnetization to reach steady state in the course of RF pulsing. If the acquisition starts with equilibrium magnetization and condition [4] is fulfilled, the resulting image intensity does not depend directly on the value of T_1. Instead of being an image-weighting parameter, T_1 becomes a *resolution* parameter. It means, under certain conditions, there will be no T_1 impact on our signal at all.

The plot of TR/T_1 for various RF pulse angle values and k-space line size N is shown in Fig. 2. The lines indicate the image blurring limits for various N. Areas below the lines correspond to the *no image blurring* zones and areas above the lines

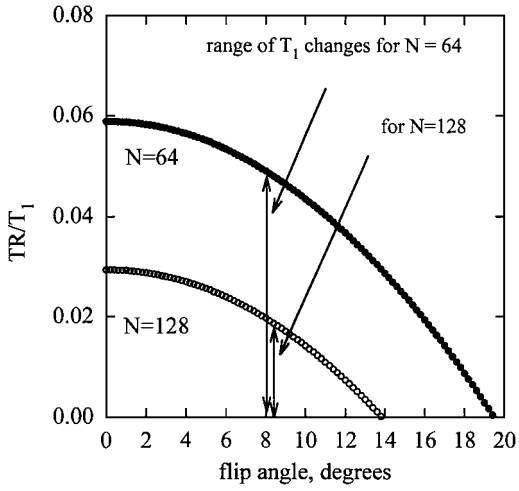

FIG. 2. The plot of TR/T_1 vs flip angle for the blurring limit $TR/T_1 = 1.2\pi/N + \ln(\cos\alpha)$ that corresponds to [4], calculated for imaging matrix sizes $N = 64$ and 128. For the area above a curve, the transient component of the magnetization causes image blurring. Note the range of TR/T_1 changes where the transient component does not influence the image resolution and there is no T_1 manifestation in the image.

correspond to the *image blurring* zones. As N increases, the pixel size becomes smaller and the no blurring zone shrinks. Having chosen our scanning parameters such as flip angle and TR, Fig. 2 helps define a range of possible T_1 changes that will not influence the image intensity during the experimental series.

Thus, we can utilize the transient state component to avoid T_1 effects, still keeping the image resolution within limits. The

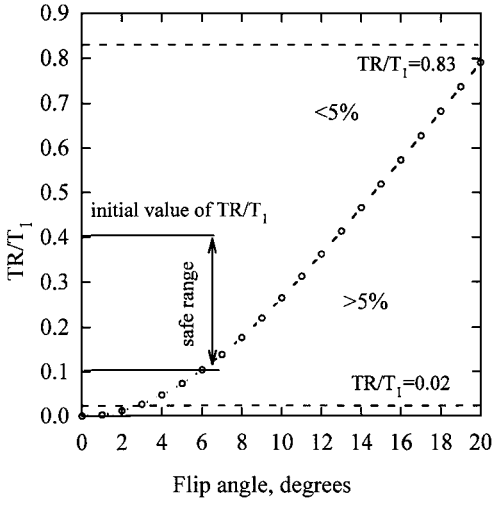

FIG. 3. The plot of TR/T_1 vs flip angle for the ratio ε of the transient and steady-state components [5] equal to 5%: $TR/T_1 = \ln(1 + (1 - \cos\alpha)/0.05)$. TR/T_1 used in imaging water-filled cuvettes were equal to 0.83 and 0.02. They are plotted in the figure as dotted lines. The areas above and below the curve give $\varepsilon < 5\%$ and $\varepsilon > 5\%$. At an initial value of $TR/T_1 = 0.4$ in our drying experiments, ε does not exceed 5% until $TR/T_1 = 0.1$. This defines the safe range of changes for T_1.

pulse angle α can be made larger than the Ernst angle, resulting in higher raw signal intensity and hence more sensitive imaging.

2.2. TR Is of the Same Order as T_1

When TR is comparable to T_1, the longitudinal magnetization recovers quickly and its transient component decays rapidly. The resolution blurring due to the transient component is quite strong, so we are deep in the blurring zone of Fig. 2. However, the image resolution depends on two separate terms: the transient component and the steady-state component. The proportion of the transient component in the observed signal can be defined from [1] as

$$\varepsilon = \frac{M_i - M_0 w}{M_0 w} = (1/w) - 1 = \frac{E(1-C)}{(1-E)} \qquad [5]$$

assuming no magnetization preparation and $M_i = M_0$.

We require no degradation of resolution and so this ratio, ε, should be small. Since we require our signal to be immune to T_1 changes, we also specify that this ratio should not change significantly. We achieve this by choosing the flip angle smaller than the Ernst angle. If the transient part of the longitudinal magnetization is much smaller than the part recovering to equilibrium, the ratio will be practically insensitive to a range of T_1 changes. Guided by experience, we have chosen an acceptable ε cut off at 5%.

In Fig. 3 we show a plot of TR/T_1 versus the flip angle for the ratio of the transient and steady-state components equal to 5%. The zone above the curve corresponds to the ratio smaller than 5%, and in the zone below the curve the ratio is larger. For a flip angle equal to 6.5° and $TR/T_1 = 0.4$, ε is smaller than 1.4%, and the "safe" range of the TR/T_1 changes starts from 0.1. For TR = 2 ms and initial value of $T_1 = 5$ ms, the signal is expected to be insensitive to T_1 changes up to 20 ms.

The Ernst flip angle for $TR/T_1 = 0.4$ is 48°. In this case, we sacrifice our signal-to-noise to make the acquired profile immune to anticipated T_1 changes.

We do not consider the case of $TR > T_1$, since in this regime the techniques espoused in this paper are either not required or not appropriate.

3. EXPERIMENTAL

Imaging experiments were performed on a Nalorac (Martinez, CA) 2.35-T 32-i.d. horizontal bore superconducting magnet, with a Tecmag (Houston, TX) Libra S-16 console. A water-cooled 7.5-cm-i.d. Nalorac gradient set (maximum gradient 100 G/cm), driven by Techron (Elkhart, IN) 8710 amplifiers, was employed. All measurements were performed at ambient temperature and humidity, using an eight-rung birdcage coil (Morris Instruments, Ottawa) driven in quadrature by a 2-kW AMT (Brea, CA) 3445 RF amplifier.

For imaging doped water cuvette phantoms, the parameters were as follows: the TR was 2 ms, encoding time t_p was 150 μs,

and number of points was 128 with a maximum gradient strength of 13 G/cm and a spatial resolution of 0.6 mm. The number of scans was four with a recovery delay between scans of 0.5 s and total acquisition time of 3 s. Four different RF pulse lengths were used, 1, 2, 3, and 4 μs, which correspond to 6.7°, 13.5°, 20.3°, and 27° rotation angles.

For demonstration experiments, a Pro-Mix BX soil (Premier Horticulture, Canada) was used. Its main components are sphagium peat moss, vermiculite, perlite, and dolomitic and calcitic limestone. The peat moss, ~80% of the volume of Pro-Mix BX, makes this a low density soil with a high porosity. The limestone acts as pH buffer, and the vermiculite and perlite add to the mineral content of the soil. Vermiculite can also add to the water uptake capability of the soil due to its mineral structure. The layered molecular sheets which make up vermiculite are padded with doubled interlayers of water molecules. These layers form when cations are present in the environment. The cations help balance charge deficiencies that exist between successive mineral layers, and also help to hold the polar water molecules in place. Such water components are in fact hydrates that have a very short T_2^* (~17 μs, (*13*)).

The one-dimensional imaging experiments were conducted on a Pro-Mix BX sample which underwent controlled drying in a humidity chamber at a set temperature. The sample was placed in a large pan and equilibrated at 97% relative humidity and 30°C environmental chamber (Caron, OH) for 14 h. Then the sample was taken out of the chamber and packed and sealed in a 25-mm (i.d.) glass tube with a teflon plug (Fig. 4). The chamber was then set at 50% relative humidity and 30°C. The drying interval between successive acquisitions was 80 min. During successive drying intervals, the sample was kept in the same glass tube, so drying proceeded only from the open end. For each profile acquisition, the sample was removed from the chamber for 50 min. Mass measurements (Mettler AE50 balance, ±0.05-mg sensitivity) indicated that negligible water loss occurred during image acquisition. The total experimental time was 21.5 h.

Bulk NMR relaxation measurements were performed on a separate Pro-Mix BX sample which was equilibrated at multiple humidities in the environmental chamber prior to measurement. The bulk sample was repacked between equilibrations.

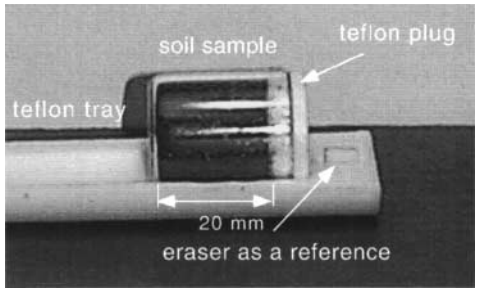

FIG. 4. A photograph of the soil sample in the glass tube with the teflon plug. The inner diameter is 25 mm and the length of the soil sample inside the tube is 18 mm. The eraser at the right serves as an image reference.

Two types of 1D SPRITE profiles, along the Z-axis, were acquired during drying: T_2^*-mapped profiles as in (*13*) and profiles with a short (40 μs) encoding time. For T_2^* mapped profiles, the imaging parameters were as follows: 2-ms TR, 7.7° flip angle, field of view was 5.5 cm with nominal resolution 0.43 mm, 64 averages. The encoding time t_p was varied from 60 to 300 μs to allow for T_2^* mapping. Thirty-six different encoding times were used. Maximum gradient values were systematically varied from 28.5 to 5.7 G/cm to keep a constant field of view in successive profiles of varying encoding.

The short encoding time acquisitions also used a 2-ms TR and 7.7° flip angle; the field of view was 6.6 cm with nominal resolution 0.5 mm, 64 averages. The 40-μs encoding time profiles were acquired to compare the validity of using a short encoding time (40 μs) against profiles produced by fitting the T_2^*-mapping data to [2].

The fitting of data was undertaken using a curve fitting routine in Interactive Data Language 5.0 (Research Systems, Inc, Boulder, CO). All experimental fits were single exponential. The fitted, T_2^*, and 40-μs encoding time profile data were plotted using SigmaPlot 4.14 (Jandel Scientific, San Rafael, CA).

4. RESULTS AND DISCUSSION

4.1. The Baseline Artifact Correction

For 1D imaging, we used the SPRITE sequence with half-k-space acquisition. We preferred starting the acquisition from the zero of k-space (no phase encoding of the first point). In this case the first point provides bulk sample information and it was very easy to control the phase adjustment of the scanner during long experimental runs. It made the acquired signal appear very similar to an FID signal in conventional NMR, with the difference being that we had *gradient evolution* due to gradient changes point to point (constant t_p, variable G) rather than *time evolution* as in a FID.

We compared two data reconstruction strategies: zero-filling to double the matrix size with consequent Fourier transform (FT) and the conjugation of the acquired half of the k-space with reconstruction of the other half and consequent echo FT. Both gave nominally doubled spatial resolution.

For the zero-filled data, their FID-like behavior was emphasized by a baseline offset artifact commonly observed in early 2D NMR experiments which also appeared in our experiment series. This artifact originates from the properties of the discrete Fourier transform (DFT). When the first data point is not displaced one half of the regular sampling interval from the center, it produces a very noticeable artifact known as "t1-ridges" (*11, 12*). Since the vertical level of a spectrum is determined by the first point of the corresponding data series, it can be eliminated by adjusting the first data point of each row in the time domain. If the first point is placed exactly at zero of the k-space

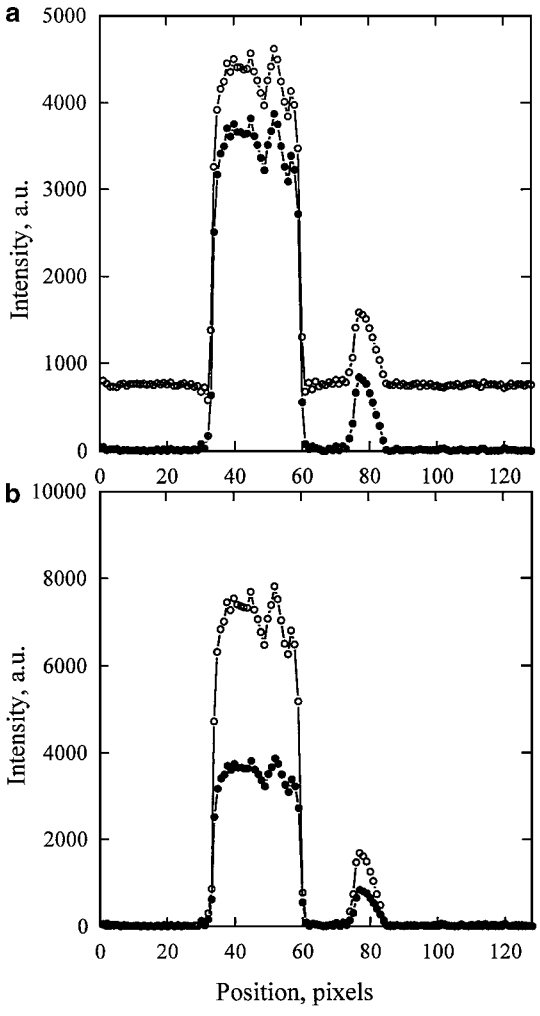

FIG. 5. The 1D profile of the soil sample for the centric SPRITE: (a) with zero-filling (○) and zero-filling with the first point correction (●); and (b) the half-k-space conjugation (○) and the zero-filling with the first point correction (●). The first point correction removes the baseline artifact completely from zero-filled data. There is no need for this correction for the conjugated data. The intensity of the latter is twice as high as that of the zero-filled data, but the signal-to-noise ratio is the same.

(when the gradients are equal to zero), the appropriate adjustment is to multiply the first point by 0.5 (*12*). In our case, the gradient list served as an analog of time, and when the first gradient value was set at zero, we faced the same problem. The above correction of the first k-space data point (multiply by 0.5) removed the baseline offset (Figs. 5a and 5b).

The profiles obtained from conjugation of the acquired half-k-space data did not have this artifact, as one can see in Fig. 5. It can be easily explained if the k-space line is imagined as a sum of two halves—to the left from zero and to the right from zero with the single common zero point. Then we can say that they are added together with their common point multiplied by 0.5, so no correction of the first point is necessary. In reconstructing the data, we preferred this method. It gives an image intensity twice as high in comparison with the zero-filled data, but the signal-to-noise ratio is naturally the same, as the number of experimental points is the same.

4.2.a. Sensitivity of the Signal Intensity to TR/T_1 Changes for Sequential and Centric SPRITE

In the centric SPRITE sequence, acquisition starts from equilibrium, and the image intensity will not be influenced by changes in T_1 (no saturation), but the ratio of the transient and steady-state components will increase with increasing T_1. For the sequential SPRITE sequence, the center of k-space is acquired when the longitudinal magnetization has reached steady state. In this case, an increase of T_1 will lead to a decrease in the signal, even for the small flip angles, because the steady-state value will decrease.

To check this experimentally, we used a doped water hemispherical phantom with T_1 equal to 22 ms. The T_2^* of the sample was 2.5 ms, so a gradient spoiler was applied at the origin of k-space to remove the residual transverse magnetization. The flip angle was set at 6.5°. The phantom, 2.5-cm o.d., was placed in the center of a 4.6-cm-i.d. birdcage probe. It was important to keep the same RF flip angle through the sample; otherwise the resulting intensity for the sequential acquisition will be averaged over the varying magnetization through the sample. To simulate the T_1 changes, the ratio TR/T_1 was altered by changing TR from 2 up to 22 ms. Both the sequential and the centric SPRITE experiments were performed.

Experimental data are shown in Fig. 6. The intensities of both sequential and centric SPRITE are normalized and plotted for different TR/T_1. One can see from the graph that the signal remains constant for the centric acquisition, while for the sequential acquisition it is changed even if the flip angle is kept

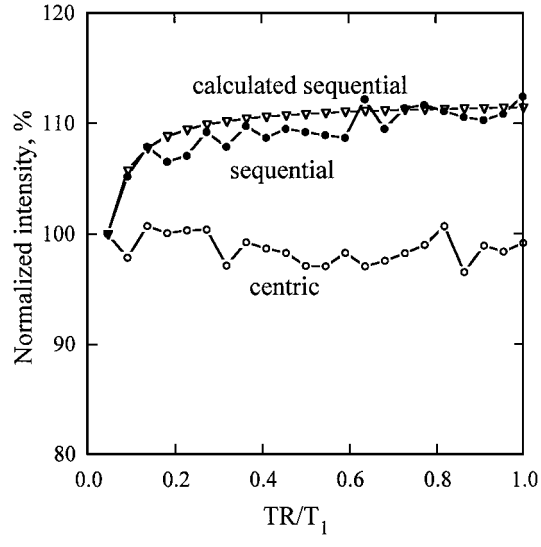

FIG. 6. The experimental signal intensity data for sequential and centric SPRITE at changing TR/T_1 for an RF flip angle 6.5°. Both the experimental (●) and the calculated (▽) intensities for the sequential SPRITE increase with increasing TR/T_1 while the experimental centric intensity (○) does not significantly change. T_1 of the sample (doped water) was 22 (±0.5) ms.

small. The experimental data for sequential SPRITE are in accordance with the calculated steady-state values of w for given parameters.

4.2.b. Signal Intensity and Resolution for Various Flip Angles at Different TR/T_1 for Centric SPRITE

As discussed in Section 2.2, T_1-weighting is not expected in the signal intensity with centric sampling. The signal should follow Eq. [2]; that is, it will be proportional to the sine of the flip angle and the initial (equilibrium) longitudinal magnetization. We can verify it by imaging samples with different T_1's at increasing flip angles. The presence of increasing T_1-weighting would produce a deviation from this linear dependence.

Although the technique is insensitive to direct T_1 changes, the signal intensity is sensitive to the ratio of transient and steady-state components. The increase of flip angle will increase the transient component blurring the resolution and possibly changing the signal intensity. To avoid this, we calculated the *safe zone* shown in Fig. 3 illustrating where changes in flip angle and TR/T_1 are tolerable.

To verify these effects experimentally, we used a set of four 1-cm^2 cuvettes filled with doped water. Cuvettes were aligned horizontally along the Z-axis of the magnet, and 1D imaging was performed in the Z-direction. All the cuvettes were filled with 0.75 g of manganese-doped water of different concentrations, so cuvettes' T_1's were 2.36, 5.80, 26.2, and 93 ms and the corresponding T_2^* were 0.222, 0.443, 1.36, and 2.41 ms with an overall precision of 2%.

The acquired profiles are shown in Fig. 7. The water menisci on the cuvette walls produce a near-parabolic image intensity.

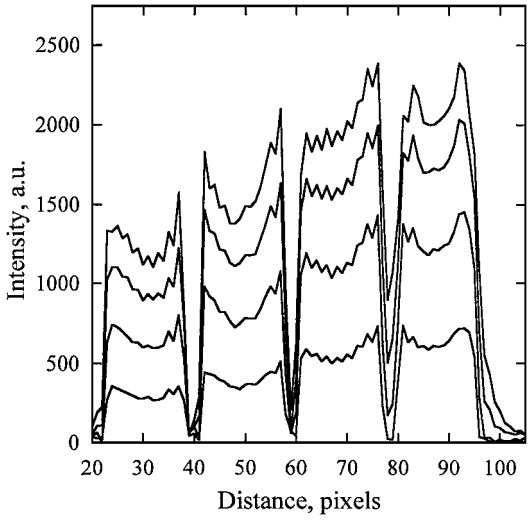

FIG. 7. 1D profiles of the doped water cuvettes at various flip angles. T_1's and T_2^*s of the water in cuvettes (from the left to the right), correspondingly: 2.4, 5.8, 26, and 93 ms and 0.22, 0.44, 1.4, and 2.4 ms. Profile intensities increase with flip angles that are 6.7°, 13.5°, 20.3°, and 27°. Notice the profile blurring of the far right cuvette with increasing flip angle. The near-parabolic shape is due to the water meniscus in each cuvette.

TABLE 1
Ratios of Normalized Signal Intensities at Different Flip Angles for Various TR/T_1's

	Flip angles			
TR/T_1	6.7(4)°	13.5(5)°	20.3(6)°	27.0(9)°
0.83	1	1.06	1.08	1.04
0.34	1	1.06	1.07	1.02
0.07	1	1.01	0.97	0.89
0.02	1	0.98	0.93	0.83

Note. Experimental accuracy was within 5% for all the data.

This image feature is maintained at all flip angle values for the first two cuvettes with shorter T_1's. This feature becomes more blurred with the flip angle increase for the cuvettes with longer (26 and 95 ms) T_1, and an increasing loss of resolution for the cuvette profiles is easily observed.

We calculated the mean value of 15 pixels over each cuvette, divided them by the sine of the corresponding flip angle, and found their ratios for various flip angles. The results are shown in Table 1. One can see that the deviations from unity become noticeable when flip angles and TR/T_1 exceed the safe zone above the line of Fig. 3. For example, at TR/$T_1 = 0.83$, we are in the safe zone at all flip angles, except for the last one. At TR/$T_1 = 0.02$, we are not in the safe zone at any flip angle. The resolution loss is accompanied by increasing deviation from the initial intensity.

The difference in signal from different cuvettes is explained by the different T_2^*'s, so to get a true proton density we normalized the cuvette intensities with corresponding T_2^* weighting [2]. The normalized profile intensities from the first three cuvettes were the same, well within the experimental accuracy. (We could not define the profile intensity from a cuvette with accuracy better than 1 pixel; in this case the accuracy was $(1/15)\times 100 = 6.6\%$.)

For the cuvette with $T_1 = 93$ ms, the intensity deviation from the other cuvettes varied from 3 to 12% at increasing flip angles. This results from blurring pixels. In the case of sequential sampling with T_1 saturation, for this cuvette the deviation would vary from 15 to 42%.

4.3. 1D Profiles of Drying Soil

To apply these methods to a practical, yet challenging drying problem in porous media, we used a Pro-Mix BX soil which is a common horticultural soil in Canada and is produced for use in greenhouses, homes, and gardens. This sample was chosen because of its microscopic heterogeneity. The NMR relaxation measurements for a Pro-Mix BX control sample are presented in Table 2. At initial humidity 97%, the water weight was 6.7% of the sample weight (Table 2). With an initial value of T_1 equal to 5 ms, we chose TR equal to 2 ms and the flip angle 7.8°. According to the above analysis, the ratio of the transient and steady-state components of the longitudinal magnetization will be insensitive to T_1 changes up to 13 ms, so the signal will be truly weighted by proton density and T_2^*, without any impact from T_1.

TABLE 2
Relaxation Time Constants for Pro-Mix

Humidity setting (%)	Water content (% w/w)	T_2^* values (μs)	T_1 values (ms)
97	6.7	700	5.5
70	4.7	504	9.7
60	4.3	207	9.0
50	3.0	155	5.6
40	1.4	138	6.4
30	1.1	130	13

Note. The T_1 values were determined using a single exponential fitting routine with 2% accuracy.

The profiles obtained with 40-μs encoding time are shown in Fig. 8a. After the extrapolation of the T_2^* mapping data, the ρ-density (Fig. 8b) and T_2^* profiles (Fig. 8c) were extracted. The product of the encoding time and the maximum gradient strength was kept as constant as possible; however, the points near the profile edges were not reliable due to slight variations of the field of view (shifts were on the order of 1–2 pixels).

The drying surface of the sample faces the reference (the 8-mm section of elastic eraser). In Fig. 8a, the signal drop-off occurs at this face prior to the rest of the sample, indicating that drying is taking place. This corresponds to changes in T_2^* profiles, where one can see the appearance of a ramp-like decrease of T_2^* as the drying progresses.

The measured mass loss during drying in the environmental chamber is shown in Fig. 9. Two different stages of drying are evident from the plotted data: the initial stage is slow and the next is more rapid. During the first half of our measurements, there is a water redistribution process inside the sample, with no significant change in proton density. There is also a slow rise of T_2^* in the middle of the T_2^* profiles that reaches its maximum at the 5th–7th time points (approx. 10–14 h of drying). The mass loss at this point is small, so it may indicate that the water redistribution takes place between the soil components.

Another noticeable feature of T_2^* profiles is that they become smoother at later times. The T_2^* falls below 200 μs, and the profiles do not show strong irregularities in T_2^* along the sample as they did at the beginning of drying. Note that the sample starts to lose water quickly at the same time.

To compare the water loss with the decrease of signal intensity, the area differences of the profiles were calculated. For the calculation of the area differences, the area of each profile was subtracted from the area of the initial profile. The mass of the sample was measured prior to each profile acquisition, and the differences between the initial mass measurement and each subsequent measurement were determined and plotted against the corresponding area differences (Figs. 10a and 10b).

If there is a direct correlation between the profile areas and the water content of the sample, it should be possible to plot a straight line regression of the change in the profile area against the corresponding change in mass of the sample. However, our encoding time range goes from 60 to 300 μs; thus, the hydrated water with short T_2^* contained in the mineral component of the soil is unobserved in both the 40-μs profiles and the T_2^*-mapped profiles. Therefore, we do not detect its evolution during drying,

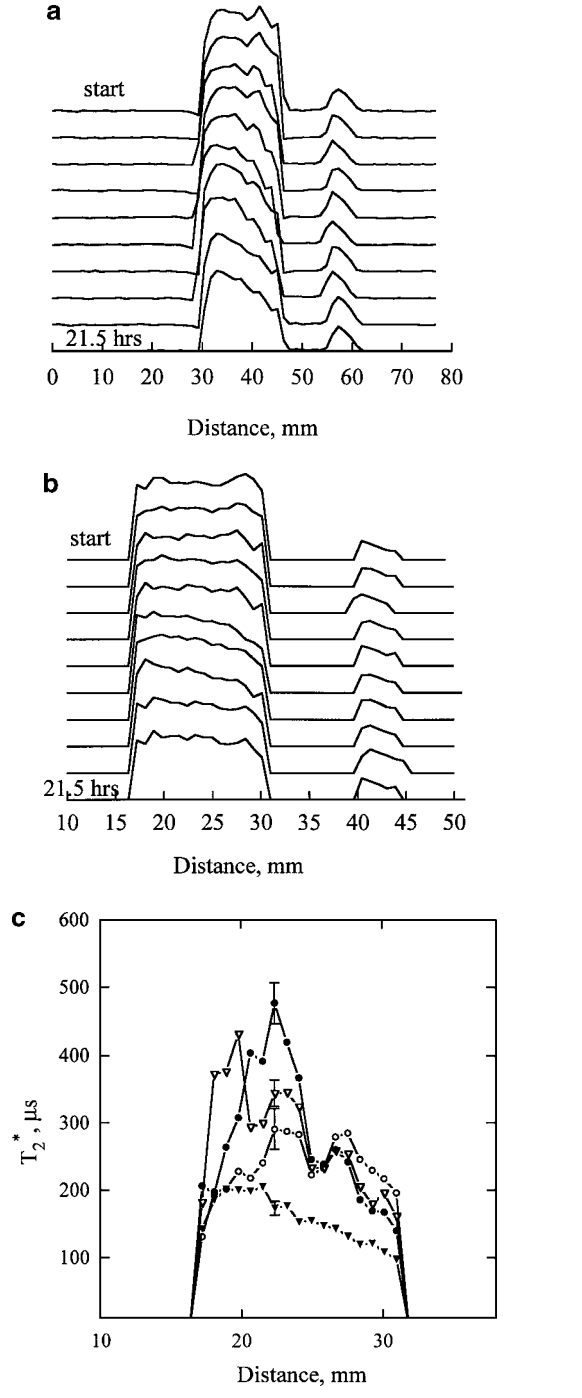

FIG. 8. The 1D profiles of the soil sample during drying: (a) the profiles acquired with 40-μs encoding time, (b) the fitted ρ-density data, and (c) T_2^* profiles for the 1st (○), 4th (●), 7th (▽), and last measurement (▼). The error of monoexponential fitting in T_2^* profiles varied from 15 (1st measurement) to 6.5% (the last measurement).

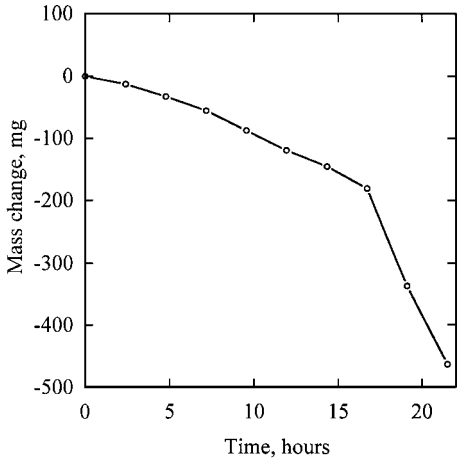

FIG. 9. The soil sample mass change (loss) during the drying due to water evaporation. Two different stages of drying are evident: the initial relatively slow stage and the final more rapid stage.

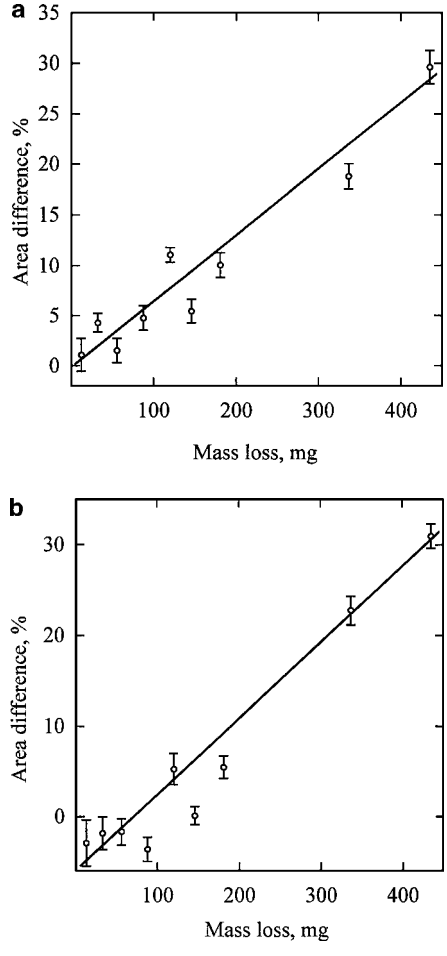

FIG. 10. The signal area differences versus the mass loss for the 40-μs encoding time profiles (a) and the ρ-density profiles (b). The experimental error for (a) varied from 62 (the 2nd point) to 1.5% (the last point). The error for the fitted profiles (b) varied from 160 (the 2nd point) to 7% (the last point).

causing this nonlinear behavior at the first stage of drying. It can also explain the lack of a clear zero intercept for the ρ-density area difference (Fig. 10b).

The linear regression works better for the late stage of drying both for the ρ-density and for the 40-μs area differences. In general, the 40-μs area difference (Fig. 10a) shows a better correlation between the water loss and the signal loss due to a shorter encoding time. It also shows that these measurements were sensitive to mass loss on the order of 25 mg.

5. CONCLUSION

We have shown that centric SPRITE can be made immune to a broad range of T_1 changes. Both for T_1 on the order of several milliseconds and on the order of hundreds of milliseconds, the signal intensity will not be saturated by T_1. Only T_2^* and the proton density manifest themselves in the signal intensity, and they can be extracted by using a simple T_2^* mapping technique. Long T_1 can result in resolution blurring.

The centric 1D SPRITE data can be conjugated with the reconstruction of the whole k-space line or zero-filled in an FID-like way. For the latter, the baseline artifact appears in the case of nonequidistant positioning of the first gradient value, and it can be easily removed.

The technique was applied to the process of drying soil with a low water content, with a Pro-Mix BX sample as an example. Proton density and T_2^* values extracted from the T_2^* mapping show that the sample loses water more or less uniformly, but T_2^* changes in a ramp-like way near the drying surface.

ACKNOWLEDGMENTS

This work was supported by equipment and operating grants awarded to BJB by NSERC of Canada. BJB also thanks NSERC for a Steacie Memorial fellowship (2000–2002). The UNB MRI Center is supported by an NSERC Major Facility Access award.

REFERENCES

1. *Geoderma* **80** (1997).
2. L. D. Hall, M. H. G. Amin, E. Dougherty, M. Sanda, J. Votrubova, K. S. Richards, R. J. Chorley, and M. Cislerova, MR properties of water in saturated soils and resulting loss of MRI signal in water content detection at 2 Tesla, *Geoderma* **80,** 431–448 (1997).
3. E. Ciampi, U. Goerke, J. L. Keddie, and P. J. McDonald, Lateral transport of water during drying of alkyd emulsions, *Langmuir* **16,** 1057–1065 (2000).
4. J. M. Salamanca, E. Ciampi, D. A. Faux, P. M. Glover, P. J. McDonald, A. F. Routh, A. C. I. A. Peters, R. Satguru, and J. L. Keddie, Lateral transport in thick films of waterborne colloidal particles, *Langmuir* **17,** 3202–3207 (2001).
5. B. J. Balcom, SPRITE Imaging of short relaxation time nuclei, *in* "Spatially Resolved Magnetic Resonance: Methods, Materials, Medicine, Biology, Rheology, Geology, Ecology, Hardware" (P. Bluemler, B. Bluemich, R. Botto, and E. Fukushima, Eds.), Wiley/VCH, Weinheim, Germany (1998).

6. B. Balcom, H. Mullally, and B. MacMillan, Proton density imaging of water migration in low water content soils, *in* "Recent Advances in MR Applications to Porous Media," October 9–11, 2000, Bologna, Italy.

7. H. Mullally, "Magnetic Resonance Imaging of Soils and Plant Roots," B.Sc. thesis, Department of Physics, University of New Brunswick, 2000.

8. I. V. Mastikhin, B. J. Balcom, P. J. Prado, and C. B. Kennedy, SPRITE MRI with prepared magnetization and centric k-space sampling, *J. Magn. Reson.* **136,** 159–168 (1999).

9. S. D. Beyea, B. J. Balcom, P. J. Prado, A. R. Cross, C. B. Kennedy, R. L. Armstrong, and T. W. Bremner, Relaxation time mapping of short T_2^* nuclei with single-point imaging (SPI) methods, *J. Magn. Reson.* **135,** 156–164 (1998).

10. C. B. Kennedy, B. J. Balcom, and I. V. Mastikhin, Three-dimensional resonance imaging of rigid polymeric materials using single-point ramped imaging with T1 enhancement (SPRITE), *Canad. J. Chem.* **76,** 1753–1765 (1998).

11. J. C. Hoch and A. S. Stern, "NMR Data Processing," Wiley-Liss, New York, 1996.

12. G. Otting, H. Widmer, G. Wagner, and K. Wuethrich, Origin of t1 and t2 ridges in 2D NMR spectra and procedures for suppression, *J. Magn. Reson.* **66,** 187–193 (1986).

13. W. P. Halperin, J.-Y. Jehng, and Y.-Q. Song, Application of spin-spin relaxation to measurement of surface area and pore size distributions in a hydrating cement paste, *Magn. Reson. Imag.* **12,** 169 (1994).